# We are IntechOpen, the world's leading publisher of Open Access books Built by scientists, for scientists

**4,800**
Open access books available

**122,000**
International authors and editors

**135M**
Downloads

Our authors are among the

**154**
Countries delivered to

**TOP 1%**
most cited scientists

**12.2%**
Contributors from top 500 universities


WEB OF SCIENCE™

Selection of our books indexed in the Book Citation Index in Web of Science™ Core Collection (BKCI)

## Interested in publishing with us?
## Contact book.department@intechopen.com

Numbers displayed above are based on latest data collected.
For more information visit www.intechopen.com

Chapter 10

# Application of Surface Plasmon Resonance Based on a Metal Nanoparticle

Amir Reza Sadrolhosseini, A. S. M. Noor and Mohd. Maarof Moksin

Additional information is available at the end of the chapter

http://dx.doi.org/10.5772/51219

## 1. Introduction

Several researchers have focused on biosensor for monitoring of biological interaction. Moreover, the detection of bimolecular is an extremely significant problem. Hence, the development of optical biosensors based on optical properties of noble metal nanoparticles using Surface Plasmon Resonance was considered.

Surface plasmon resonance (SPR) is a powerful technique to retrieve information on optical properties of biomaterial and nanomaterials. Biosensor based on SPR is a versatile technique for biological analysis applications. Essentially, SPR depends on the optical properties of metal layer [1] and enviromental changes so it is related to charge density oscillation at the interface between them [2]. Hence, biomolecular possess an extreme sensitivity to plasmon resonance and they remove the requirement for extrinsic biomolecular labeling [3]. One advantage of SPR is, the light beam never passes through the dielectric medium of interest and hence the effect of absorption of the light in the analyte can be ignored. Hence, the main potential of surface plasmon resonance is characterization of medium after the metal layer.

Sometimes polymer layer was coated on gold later for detection and improvement the sensor performence. So, the properties of nanostructures gave rised to interest in biosensing. Nano particles and Nano tube have improved the sensitivity, selectivity, and multiplexing capacity in biosensors. Different types of nanostructure-based biosensors including carbon nanotube, $SnO_2$ nanoparticles, nanowires, and nanogap biosensors have emerged..

Biomolecular interaction are determined and predicted via angular modulation sensor; hence, the out put of SPR biosensor sensor is angle shift ($\theta_{spr}$), associated with the point of minimum reflected light intensity and is very sensitive to the changes in the dielectric constant of the medium. So, the sensitivity of modern SPR sensing systems based on the Kretschmann configuration is such that they are capable of detecting refractive indexes as

high as approximately $5 \times 10^{-7}$ refractive index units, which corresponds to a 1 pg/mm$^2$ surface coverage of biomolecules [4, 5].

Unfortunately, when sensing biomolecules of low molecular weight or in low concentration, the variation in SPR angle is very small and this causes difficulties in detecting the acquired signal [6]. Hence, several researchers have focused on enhancement of sensitivity of biomolecular sensor. Hence, the properties of metal nanoparticles (gold and silver) have contemplate as a result of the physical characteristics of surface-enhanced Raman scattering (SERS). Zhu at al., (1998) utilized colloidal gold nanoparticle films to enhance the the Raman scattering of the underlying molecules [7]. On the other hand the colloidal gold nanoparticles were used as a immobilized element on the thin gold film[8, 9]. Moreover, to improve the roughness of the film, the inclusion of colloidal Au nanoparticles was added to the gold film. SPR biosensors using colloidal Au-modified gold films has the large angle shift and increase in minimum reflectivity suggesting that SPR spectrum depend on size and volume fraction of the Au nanoparticles [10]. To improve the detection of SPR biosensors, He et al., (2000)[11] and; Lyon et al., (1998)[10] reported using biomolecule-tagged colloidal Au nanoparticles. In this case, the SPW damped strongly because the intraction of the biomolecules -colloidal Au were occouured with the immobilized bio-monolayer sensing. However, using this method to generate a biomolecular interaction signal involves complex procedures for the preparation of nano-sized colloidal Au particles and chemical immobilizations to tag the biomolecules. This process, eliminates the major advantage of SPR technology, namely that biomolecular labeling is not required [6]. On the methods for improving the the sensitivity of SPR biosensors was reported by Gestwicki et. al. [12]. They enhanced the sensitivity and response of biosensor based on absorption spectroscopy techniques [13, 14]. They shown the resonance angle can be improved by caused by the conformational changes of proteins and enzymes when they bind with analytes of low molecular weights and the response of sensor can be increased by adopting Au nanoshells or nanoclusters.

The Au nanocluster-embedded dielectric film is fabricated through a simple co-sputtering method utilizing a multi-target sputtering system. In the proposed method, the resolution of the SPR biosensor is enhanced by precisely regulating the size and volume fraction of the Au nanoclusters in order to control the surface plasmon effect [6].

Carbon nanotubes (CNTs)[15] have been used as both electrode and transducer components in biosensors becuse of their interesting electrochemical and electrical properties including thier flexibility for varying the electrical property (from metallic to semiconductor) and their, small diameters, high mechanical strength, and easy fabrication/integration. Wang [16] and Balasubramanian and Burghard [17], presented the design methodologies, performance characteristics, and potential applications of CNT biosensors, as well as the factors limiting their practical use. It is obvious that many challenges still do remain, especially regarding the sensitivity of the nanotube response to environmental effects, and also the chosen type of raw CNT material, and its functionalization.

The other nanostructured sensors is based on nano ceramic such as $ZnO$ and $SnO_2$. For example, the $SnO_2$ sensor has demonstrated a potential for gas sensing applications. Liu et al. [18] developed a highly sensitive and nanostructured $SnO_2$ thin-film sensor for the detection of ethanol vapor. Its lower LOD (below 1 ppm) demonstrates an improvement over that of other works reported in the literature. Recently, Choi et al. [19] implemented a functionalized $ZnO$ nanowire field effect transistor (FET) biosensor for the low level detection of biomolecular interactions. This biosensor was fabricated without any doping which showed an enhanced sensitivity compared to other nanowire biosensors.

Fundamentally, the base of the biosensor is the coupling of a ligand-receptor binding reaction [1] to a signal transducer. Moreover, angular, phase and polarization modulations are the various methods applicable for distinguishing the interaction of bimolecular with the receptor. Essentially, SPR is a quantum electromagnetic phenomenon that appears at the interface of the dielectric and the metal. Under certain conditions, the energy of the light beam is absorbed by collective excitation of the free electrons called surface Plasmon (SP), which lies between the interface of the dielectric and the metal. On the other hand, when the momentum of the photon matches that of the Plasmon, the resonance appears as an interface of two two media with dielectric constants of opposite signs, and the SP wave propagates along the interface. In accordance with the SP wave properties, the SPR is classified as propagating the SPR, the long-range SPR and the localized SPR.

In the case of propagating SPR (PSPR) [20], the amplitude of the SP wave is decaying exponentially normal to the interface, which the Plasmon propagates, for a distance of about one to ten microns. The interactions between the surface and molecules in the analyte lead to the SPR signal shift which can be observed in shift of the angle of resonance and the wavelength. A second type of Plasmon's wave is Long-range SPR (LRSPR) that occurs in thin metal films with low attenuation; hence, the traveling distance of the Plasmon wave is about a millimeter in the visible range.

The localized SPR (LSPR) [20, 21] is exited on a nano-scale. On the other hand, the LSPR appears in the metal structure as a lateral size that is less than half the wavelength of the excitation photon. Hence, the light beam will interacts with the nanoparticles, so as to leads to a locally Plasmon oscillation occurring around the particle with a specific frequency similar to LSPR. However, the LSPR is more sensitive to changes in the local dielectric analyte [20]. Typically, researchers will measure the changes in the local dielectric environment or analyte via making shifts in the LSPR wavelength measurements. Moreover a variant of angle-resolved sensing that is possible for LSPR is also possible, and LSPR can provide real-time kinetic data for the binding processes. In addition, the PSPR signal is more sensitive to changes in the bulk refractive index than are the LSPR signals, so when the LSPR and PSPR signals are examined the interaction with the molecular adsorption layer and, the response of the two methods becomes comparable in the short-range[20]. Consequently, both sensitivity and flexibility are the capability of the LSPR. Moreover, the decay length is shorter than PSPR; hence, the LSPR are offered for the sensor.

## 2. Optical properties of metal

Assume that the material such as metal consist of charges which can be set in motion by an oscillating electric field of light that is polarized in one direction. In accordence with Newton's second law of motion, displacement of the electron and damping factor which is a function of mass of electron and relaxation time, the polarization density ($P_c$) of the conduction electrons is given as

$$P_c = -nex_0(t) = -\frac{ne^2\tau}{m_e\omega}E\frac{\omega\tau - i}{\omega^2\tau^2 + 1} \tag{1}$$

where $x_0(t)$ , $m_e$ and $\tau$ are the displacement , mass of electron respectively and a decay or relaxation time [2]. Hence, the total polarization is

$$P = P_b + P_c \tag{2}$$

Wher $P_b$ is the background polarization, and the susceptibility ( $\chi = \frac{P}{E}$ ) therefore the dielectric function ($\varepsilon$) is

$$\varepsilon = 1 + 4\pi\chi \Rightarrow \varepsilon = 1 + 4\pi\frac{P_b + P_c}{E} \tag{3}$$

By using the equations (1-3) the dielectric function can be written as [2, 21],

$$\varepsilon = 1 + \frac{4\pi P_b}{E} - \frac{4\pi ne^2\tau}{m_e\omega}\cdot\frac{\omega\tau - i}{\omega^2\tau^2 + 1} \tag{4}$$

or

$$\varepsilon = \varepsilon' - i\varepsilon'' \tag{5}$$

In the case of high frequency of $\omega \to \infty$

$$\varepsilon_\infty = 1 + \frac{4\pi P_b}{E} \tag{6}$$

Then by using equations (4) and (6),

$$\varepsilon = \varepsilon_\infty - \frac{4\pi ne^2\tau^2}{m_e(\omega^2\tau^2 + 1)} + \frac{4\pi ne^2\tau}{\omega\ m_e(\omega^2\tau^2 + 1)}i \tag{7}$$

Two frequency regimes of interest in equation (7) are to be considered for studying the material response [2].

i. Low frequency regime

For the case of the frequency $\omega$ is less than $1/\tau$, $\varepsilon'' = 4\tau\pi ne^2/(\omega m_e)$ the real terms of equation (7) can be neglected [2]. In this case the media is absorbent and the absorption coefficient ($\alpha$) is

$$\alpha = \frac{\omega}{c}\sqrt{2\varepsilon''} \ , \ \alpha = \frac{\omega}{c}\sqrt{\frac{8\pi n e^2 \tau}{m_e \omega}} \tag{8}$$

ii. High frequency regime

Since the dielectric function is real in the high frequency regime, the imaginary part of Eq. (7) can be ignored. In this case the frequency $\omega$ is more then $1/\tau$, the dielectric function is therefore,

$$\varepsilon = \varepsilon_\infty - \frac{4\pi n e^2 \tau^2}{m_e(\omega^2\tau^2 + 1)} \tag{9}$$

or,

$$\varepsilon = \varepsilon_\infty (1 - \frac{\omega_p^2}{\omega^2}) \tag{10}$$

Where, the plasma frequency ($\omega_p$) is defined as

$$\omega_p = \frac{4\pi e^2 n}{\varepsilon_\infty m_e} \tag{11}$$

As can be seen from equation (10) the dielectric function vanishes at the plasma frequency. However, for $\omega > \omega_P$ the medium behaves like non-absorbing and the light beam traverses through the medium without attenuation. On the other hand when $\omega < \omega_P$, the medium is of high reflectivity behaviour. Therefore the plasma frequency is the frequency of collective oscillations of the electron gas (plasma). The electron density oscillates at the plasma frequency and plasma oscillations are longitudinal type excitation [2]. The quantum of the plasma oscillation is called *plasmon* which can be excited by X ray and light or by an inelastic electron scattering [22].

To obtain the conditions of excitation to result in resonance, let's consider the electrical field component in the *x* direction,

$$\vec{E} = \vec{E} e^{i(k_x x - \omega t)} e^{-\alpha z} \tag{12}$$

where $\alpha$ is the absorption coefficient and $k_x$ is the wave number. The absorption coefficients and dielectric constants of two adjacent media is related by

$$\frac{\alpha_1}{\alpha_2} = -\frac{\varepsilon_1}{\varepsilon_2} \tag{13}$$

By using the transverse wave equation ( $\nabla^2 \vec{E} = \frac{\varepsilon}{c^2}\frac{d^2\vec{E}}{d^2 t}$ ) on the components of the electrical field, a dispersion relation for surface plasmon can be obtained as

$$k^2{}_{palasmon} = \frac{\omega}{c}\left[\frac{\varepsilon_1 \cdot \varepsilon_2}{\varepsilon_1 + \varepsilon_2}\right] \tag{14}$$

The plot of this equation is shown in Figure 1a. In the figure the wave number of the surface plasmon wave is always larger than the photon wave number and hence the photon would not be able to excite surface plasmon. The dispersion curve of the photon and surface plasmon wave must cross each other as shown in Figure 1.b [2, 20] for surface plasmon resonance to occur when the momentum of incoming light is equal to momentum of the plasmons. This can be done by using prism coupling method as in the present work.

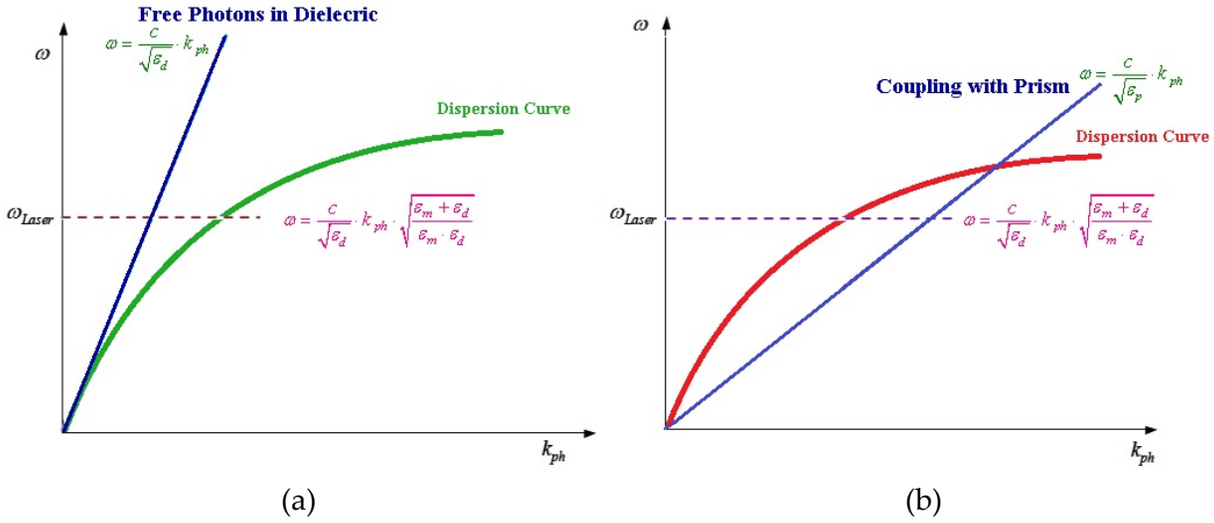


**Figure 1.** a) The wave number of photon is always less than the wave number of Plasmon at all frequencies and b) The wave number of photon may equal the wave number of number of plasmon.

## 3. Optical properties of the metal nano particles

The nanoparticles of interest are typically large enough to accurately apply classical electromagnetic theory to describe their interaction with light [23, 24]. However, they are also small enough to allow observation strong variations in the optical properties depending on the particle size, shape, and local environment. Because of the complexity of the systems being studied, efficient computational methods are the capable of treating large size materials are essential. In the past few years, several numerical methods have been developed to determine the optical properties of small particles, including the discrete dipole approximation (DDA) [23], T-matrix, and spectral representation methods (SR) [25]. We employed the DDA, which is a computational procedure suitable for studying the scattering and absorption of electromagnetic radiation by particles with sizes in the order or less of the wavelength than the incident light. DDA has been applied to a broad range of problems, including interstellar and interplanetary dust grains, ice crystals in the atmosphere, human blood cells, surface features of semiconductors, metal nanoparticles and their aggregates, and more. The DDA was first introduced by Purcell and Pennypacker [26]

and has been subjected to several improvements, in particular those made by Draine et. al [27]. Below, we briefly describe the main characteristics of DDA and its numerical implementation, namely, the DDSCAT cod[1]. For a full description of DDA and DDSCAT [23], the reader can consult refs [24-28].

The main idea behind DDA is to approximate a scatter, in our case the nanoparticle, by large enough array of polarizable point dipoles. Once the location and polarizability of each dipole are specified, the calculation of the scattering and absorption efficiencies by the dipole array can be determined, depending on the accuracy of the mathematical algorithms and the capabilities of the computational hardware. Although the calculation of the radiated fields in DDA is, in theory and principle, also possible, that calculation is actually beyond the computational capabilities of any of the current systems.

Let us assume an array of $N$ polarizable point dipoles located at $\{r_i\}$, $i$ = 1, 2, ..., $N$, each one characterized by a polarizability $\alpha_i$. The system is excited by a monochromatic incident plane wave $E_{inc}(r,t) = E_0 e^{ik.r-i\omega t}$ where $r$, $t$, $\omega$, $k = \omega/c = 2\pi/\lambda$, $c$ and $\lambda$ are the position vector, time, the angular frequency, the wave vector, the speed of light and the wavelength of the incident light. Each dipole of the system is subjected to an electric field that can be split in two contributions: (i) the incident radiation field, plus (ii) the field radiated by all of the other induced dipoles. The sum of both fields is the so-called local field at each dipole and is given by

$$E_{i,loc} = E_{i,inc} + E_{i,dip} = E_0 e^{ik.r_i} - \sum_{i \neq j} A_{ij}.P_j \tag{15}$$

where $P_i$ is the dipole moment of the $i$th element, and $A_{ij}$ with $i \neq j$ is an interaction matrix with $3\times3$ matrixes as elements, such that [23]

$$\vec{A}_{ij}.\vec{P}_i = \frac{e^{ikr_{ij}}}{r_{ij}^3}\left\{k^2\vec{r}_{ij}\times(\vec{r}_{ij}\times\vec{P}_j) + \frac{(1-ikr_{ij})}{r_{ij}^2}\left[r_{ij}^2\vec{P}_j - 3\vec{r}_{ij}(\vec{r}_{ij}.\vec{P}_j)\right]\right\} \tag{16}$$

Here $r_{ij} = \left|\vec{r}_i - \vec{r}_j\right|$, and $\vec{r}_{ij} = \vec{r}_i - \vec{r}_j$, and we are using *cgs* units. Once we solve the 3$N$-coupled complex linear equations given by the relation

$$\vec{P}_i = \alpha_i.\vec{E}_{i,loc} \tag{17}$$

and determined each dipole moment $\vec{P}_i$, we can then find the extinction and absorption cross sections for a target, $C_{ext}$ and $C_{abs}$ in terms of the dipole moments as [23]

$$C_{ext} = \frac{4\pi k}{\left|\vec{E}_0\right|^2}\sum_{i=1}^{N}(\vec{E}^*_{i,inc}.\vec{P}_i) \tag{18}$$

[1] Discrete Dipole Scattering (DDSCAT) is a Fortran code for simulation and calculation of scattering and absorption of light by particles.

$$C_{abs} = \frac{4\pi k}{\left|\vec{E}_0\right|^2} \sum_{i=1}^{N} \left\{ \mathrm{Im}\left[ \vec{P}_i . (\alpha_i^{-1})^{\dagger} P_i^{\dagger} \right] - \frac{2}{3} k^3 \left|P_i\right|^2 \right\} \tag{19}$$

where † means complex conjugate. The scattering cross section can be obtained using the following relation:

$$C_{ext} = C_{sca} + C_{abs} \tag{20}$$

Certain arbitrariness in the construction of the array of dipole points represents a solid target of a given geometry. For example, the geometry of the grid where the dipoles have to be located is not uniquely determined, and a cubic grid is thus usually chosen. Also, it is not obvious how many dipoles are actually required to adequately approximate the target or which choice is the best for the dipole polarization. If one chooses the separation between dipoles $d$ such that $d \ll \lambda$ , then one can assign the polarize for each particle $i$ in a vacuum, using the lattice dispersion relation (LDR) polarization, $\alpha_i^{LDR}$ at a third order in $k$ , given by [23, 27]

$$\alpha_i^{LDR} = \frac{\alpha_i^{CM}}{1 + \alpha_i^{CM} \left[ b_1 + b_2 \varepsilon_i + b_3 S \varepsilon_i \right] (k^2 / d)} \tag{21}$$

where $\varepsilon_i$ is the macroscopic dielectric function of the particle, $\alpha_i^{CM}$ is the polarizability given by the well-known Clausius- Mossotti relation

$$\alpha_i^{CM} = \left( \frac{d}{3} \right)^3 \frac{\varepsilon_i - 1}{\varepsilon_i + 2} \tag{22}$$

and $S$ , $b_1, b_2$ and $b_3$ are coefficients of the expansion. Now the question is, how many dipoles do we need to mimic the continuum macroscopic particle with an array of discrete dipoles? The answer is not straightforward, because we have to consider the convergence of the physical quantities as a function of the dipole number. It has been found that $N \geq 10^4$ for an arbitrary geometry is a good starting number, as shown in the Appendix. However, we do have a matrix of $(3N)^2$ complex elements that require a large amount of computational effort. In this work, we have employed the code adapted by Draine and Flatau to solve the complex linear equations found in DDA. To solve the complex linear equations directly would require tremendous computer capabilities; however, one can use iterative techniques to compute the vector $\vec{P} \equiv \left\{ \vec{P}_i \right\}$. In this case, each iteration involves the evaluation of matrix-vector products such as $\vec{A}.\vec{P}^{(n)}$ , where $n$ is the number of the iteration. The algorithm, named DDSCAT, locates the dipoles in a periodic cubic lattice, and then uses fast Fourier transform techniques to evaluate matrix-vector products such as $\vec{A}.\vec{P}$ , which thus allows the whole computation of the final vector $\vec{P}$ for a large number of dipoles [28]. For a detailed description of DDA and DDSCAT code, the reader can look at refs [24-28].

In 2003, Sosa et. al. [23] defined the extinction, absorption and scattering efficiencies or coefficients, $Q_{ext}$, $Q_{sca}$ and $Q_{abs}$ as

$$Q_{ext} = \frac{C_{ext}}{A},\ Q_{abs} = \frac{C_{abs}}{A},\ Q_{sca} = \frac{C_{sca}}{A} \tag{23}$$

Where $A = \pi a_{eff}^2$ and $a_{eff}$ is/are defined through the concept of an effective volume equal to $4\pi a_{eff}^3 / 3$.

In Figure 2 [23], we show $Q_{ext}$, $Q_{sca}$ and $Q_{abs}$ in dotted, dashed, and solid lines, respectively, as a function of the wavelength of the incident light, $\lambda$ for nanometric-sized particles. The calculations were done for nanoparticles with $a_{eff} = 50nm$ and dielectric functions as measured on bulk silver and gold by Johnson and Christy [29]. The nanoparticles were represented or mimic by around 65000 point dipoles in order to have a good convergence on their optical properties, as discussed below. The number of these dipoles is quite large in comparison with the numbers used in previous studies on isolated and supported small metallic nanoparticles [30, 31] where, incidentally, only an extinction efficiency was reported. Our use of a large number of dipoles is in agreement with the results found in a previous study where we learned that even for small metallic nanoparticles with radii of about a few nanometers, one needed more than 12000 dipoles to achieve convergence on their optical properties [32]. A larger number of dipoles is necessary to achieve that convergence. In particular, we found that extinction efficiency converges very rapidly as a function of the number of dipoles. However, this is not the case for the absorption or scattering efficiencies where a very large number of dipoles were necessary to achieve that convergence. It is also well known that for small nanoparticles *(<20 nm*) the light absorption process dominates the extinction spectrum, whereas for very large nanoparticles *(>100 nm*), the light-scattering process dominates. As we show in this paper, to elucidate the optical properties of medium-size nanoparticles, it is indispensable to undertake an in-depth study of the scattering and absorption efficiencies, and not only of the extinction one, because both phenomena, namely, scattering and absorption, are the same order of magnitude. Figure 2 shows the optical efficiencies for a sphere with a radius of *50 nm*. In the spectra, we can observe that at about *320 nm* all the efficiencies have a local minimum that corresponds to the wavelength at which the dielectric functions of silver. Therefore, this feature of the spectra is inherent to the material properties and, as we observe below, that feature independent of the particle geometry. Below *320 nm*, the absorption of light is mainly due to the intra-band electronic transitions of silver; therefore, this feature of the spectra should also be quite independent of the shape and size of the particles, as it is actually corroborated in all of the graphs shown below that corresponding to a silver particle. At about 350 nm, the spectrum of $Q_{abs}$ shows a peak is related to the excitation of the surface Plasmon of the sphere; therefore, this feature is inherent to the geometry of the particle, although the position depends on its material properties. At larger wavelengths the spectrum of $Q_{abs}$ shows specific features from *380 nm* to about *500 nm* that corresponds to plasmon excitations due to higher multi-polar charge distributions [23]. If we look only at the $Q_{ext}$, it is not possible to observe the same features because scattering effects hide them. The $Q_{sca}$

spectrum shows a broad structure from *320 nm* to *750 nm*, with a maximum being about *400 nm*, three times more intense than the maximum of $Q_{abs}$ . The characteristics of the $Q_{sca}$ spectrum are mainly due to the size of the particle. In a previous work [33], we found that this maximum is less pronounced as the radius of the sphere increases. Also, the $Q_{sca}$ spectra of nanospheres decay slowly as the radius increases, which means that as the sphere becomes larger it scatters light at longer wavelengths, just as expected. The long tail in the extinction spectrum corresponds to Rayleigh scattering which also observed in the extinction spectra shown below.

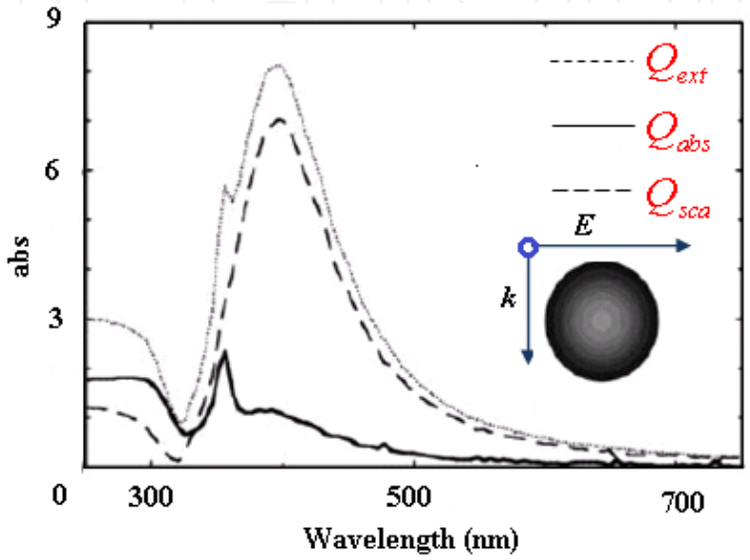


**Figure 2.** Optical coefficients for a silver nanosphere[23]

## 4. Theory

### 4.1. Surface plasmon resonance with prism coupling

We study SPR in the classical Kretschmann's configuration shown in Figure 3, where one side of the glass prism is coated thin gold or silver film in contact with the probed sample. Surface plasmons, which are collective oscillations of free electrons, are propagating along the interface between the sample and the metal film, and are thus sensitive to the optical properties of both the sample and the metal film. These plasmons can only be excited with TM-polarized light, which has an electric field component normal to the surface that generates the required surface charge distribution for the excitation [34].

The incident light is totally internally reflected at the interface and its intensity decreases with incident angle which is also called as coupling angle. By using the momentum and energy conservation laws [1, 35] the condition of resonance is obtained as follows:

$$k_{glass} \sin\theta_i = \frac{\omega}{c} n_{glass} \sin\theta_i = k_{plasmon} \tag{24}$$

where $\theta_i$ is the coupling angle.

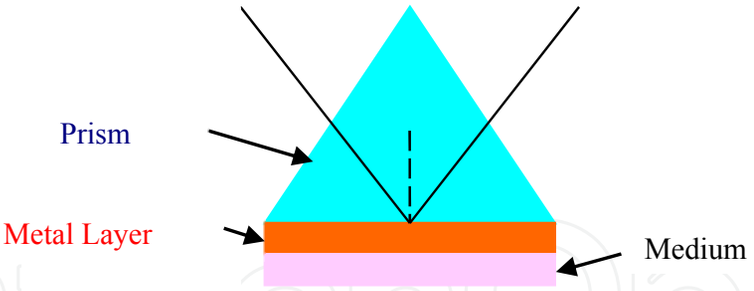


**Figure 3.** Kretschmann configuration

To excite the SPW the electrical and magnatisam fields are parallel and perpendicular in the incident plane which is defined by light propagation vector and the normal to the interface. Thus, in accordance with Figure 4 and the boundary conditions, the relationship between electrical and magnetism fields can be written as follows [2, 22]:

$$B_a = n_0\sqrt{\varepsilon_0\mu_0}(E_0 + E_{r1}) = n_1\sqrt{\varepsilon_0\mu_0}(E_{t1} + E_{i1}) \tag{25}$$

$$B_b = n_1\sqrt{\varepsilon_0\mu_0}(E_{i2} + E_{r2}) = n_2\sqrt{\varepsilon_0\mu_0}E_{t1} \tag{26}$$

$$E_a = (E_0 - E_{r1})\cos\theta_0 = (E_{t1} - E_{i1})\cos\theta_{t1} \tag{27}$$

$$E_b = (E_{i2} - E_{r2})\cos\theta_{t1} = E_{t2}os\theta_{t2} \tag{28}$$

The relationship between $E_a$, $B_a$ and $E_b$, $B_b$ are obtained by using phase change due to light passing through the different layers and $E_{i1} = E_{r2}e^{-i\delta}$, $E_{i2} = E_{t1}e^{-i\delta}$, $B_{i1} = B_{r2}e^{-i\delta}$, $B_{i2} = B_{t1}e^{-i\delta}$, $B = \frac{n}{c}E$ and $c = \frac{1}{\sqrt{\varepsilon_0\mu_0}}$ [2, 22], as follows [36]:

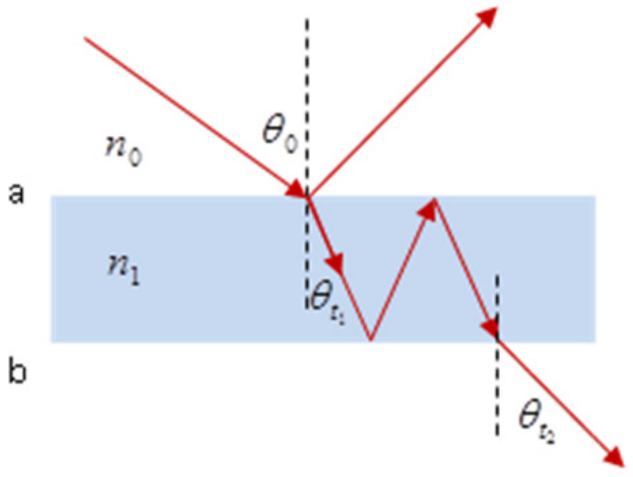


**Figure 4.** Reflection and refraction at the interface

$$E_a = (e^{-i\delta}\cos\delta)E_b - (i\frac{e^{-i\delta}}{\tau_1}\sin\delta)B_b \tag{29}$$

$$B_a = (-\tau_1 ie^{-i\delta}\sin\delta)E_b + (e^{-i\delta}\cos\delta)B_b \tag{30}$$

as $\tau_n$ is

$$\tau_N = \frac{n_N}{\cos\theta_{t_N}}\sqrt{\varepsilon_0\mu_0} \tag{31}$$

Consequently, the layers cause the phase change of light and the matrix layers obtain from the coefficient of equations (30) and (31) as follows:

$$\begin{bmatrix} E_a \\ B_a \end{bmatrix} = M\begin{bmatrix} E_b \\ B_b \end{bmatrix}$$

where $M$ is a matrix consist of

$$M = \begin{bmatrix} \cos\delta & -i\dfrac{\sin\delta}{\tau_1} \\ -i\tau_1\sin\delta & \cos\delta \end{bmatrix}, \tag{32}$$

where $\delta$ is the phase shift due to the beam passing through different layer given as

$$\delta = \frac{2\pi}{\lambda}dn_1\cos\theta_{t_1} \tag{33}$$

where $d$ is the thickness of layer. Considering more than one layer is involved for description and simulation of SPR, the matrix for N-layer can be achieved from the relation between tangential fields at the boundary of the first layer up to the $N_{th}$ layer as follows [2, 36, 37]

$$\begin{bmatrix} E_a \\ B_a \end{bmatrix} = M_1M_2M_3.....M_N\begin{bmatrix} E_b \\ B_b \end{bmatrix} \tag{34}$$

Substituting,

$$M = M_1M_2M_3.....M_N \tag{35}$$

and the characteristic matrix [ 38] is

$$M = \begin{bmatrix} m_{11} & m_{12} \\ m_{21} & m_{22} \end{bmatrix} \tag{36}$$

If one layer is deposited on the prism, the reflection and transmission coefficients are defined respectively as

$$r = \frac{E_{r_1}}{E_0} \tag{37}$$

and

$$\Gamma = \frac{E_{t_2}}{E_0} \tag{38}$$

and from equations (25, 26, 27, 28 and 36), it can be obtained that

$$\begin{bmatrix} (E_0 - E_{r_1})\cos\theta_0 \\ n_0\sqrt{\varepsilon_0\mu_0}(E_0 + E_{r_1}) \end{bmatrix} = \begin{bmatrix} m_{11} & m_{12} \\ m_{21} & m_{22} \end{bmatrix} \begin{bmatrix} E_{t_2}\cos\theta_{t_1} \\ n_2\sqrt{\varepsilon_0\mu_0}E_{t_2} \end{bmatrix} \tag{39}$$

By substituting equations (37 and 38) in equation (39) and after simplification, the reflection coefficient is as follows:

$$r = \frac{m_{21} + m_{22}\tau_2 - m_{11}\tau_0 - m_{12}\tau_2\tau_0}{m_{21} + m_{22}\tau_2 + m_{11}\tau_0 + m_{12}\tau_2\tau_0} \tag{40}$$

whereby the reflectivity is

$$R = rr^* \tag{41}$$

If there are three media of prism, $n_0$, metal layer, $n_1$ and air ($n_2 = 1$); and the thickness of metal layer, $t$, is less than wavelength ($\lambda = 632.8nm$) then the characteristic matrix is

$$M = \begin{pmatrix} 1 & -i(2\pi/\lambda)d\cos^2\theta_{t1} \\ -i(2\pi/\lambda)dn_1^2 & 1 \end{pmatrix} \tag{42}$$

According to equations (37, 40) and (41), the reflection coefficient is

$$r = \frac{\overbrace{\left(\tau_0 n_2\sqrt{\varepsilon_0\mu_0} - \cos\theta_{t_2}\right)}^{A} - i\overbrace{\alpha\left(n_1^2\cos\theta_{t_2}\tau_0 - \cos^2\theta_{t_1}\sqrt{\varepsilon_0\mu_0}\right)}^{B}}{\underbrace{\left(\tau_0 n_2\sqrt{\varepsilon_0\mu_0} + \cos\theta_{t_2}\right)}_{C} - i\underbrace{\alpha\left(n_1^2\cos\theta_{t_2}\tau_0 + \cos^2\theta_{t_1}\sqrt{\varepsilon_0\mu_0}\right)}_{D}} \tag{43}$$

Substituting $\alpha$ for $2\pi t/\lambda$, and after multiplying the numerator and denominator of equation (42) with the complex conjugate of the denominator, the reflection coefficient is derived as follows:

$$r = \frac{AC + \alpha^2 BD - i\alpha(BC - DA)}{C^2 + \alpha^2 D^2} \tag{44}$$

and the phase change [39] is

$$\tan\phi = \frac{\alpha(BC - DA)}{AC + \alpha^2 BD} \tag{45}$$

## 4.2. Theory of localized SPR

In a general and simple case, we can assume that the nanoparticle is as metallic sphere with the radius R. It is embedded in a liquid medium. So, the SP wave just can propagate less than the 100 nm or the size of particle; hence, becomes localized.

The electrical field outside the sphere is [20]:

$$E_{out}(x,y,z) = E_0\hat{z} - \left|\frac{\varepsilon_m - \varepsilon_d}{\varepsilon_m + 2\varepsilon_d}\right| \times a^3 E_0 \left[\frac{\hat{z}}{r^3} - \frac{3z}{r^5}(x\hat{x} + y\hat{y} + z\hat{z})\right] \quad (46)$$

where $E_0$ is the applied field magnitude polarized in the $z$ direction. The free electron clouds are dislocate by the electromagnetic wave field and produces uncompensated charges near the particle surface which produces corresponding opposing forces (as in Figure 5 [20]).

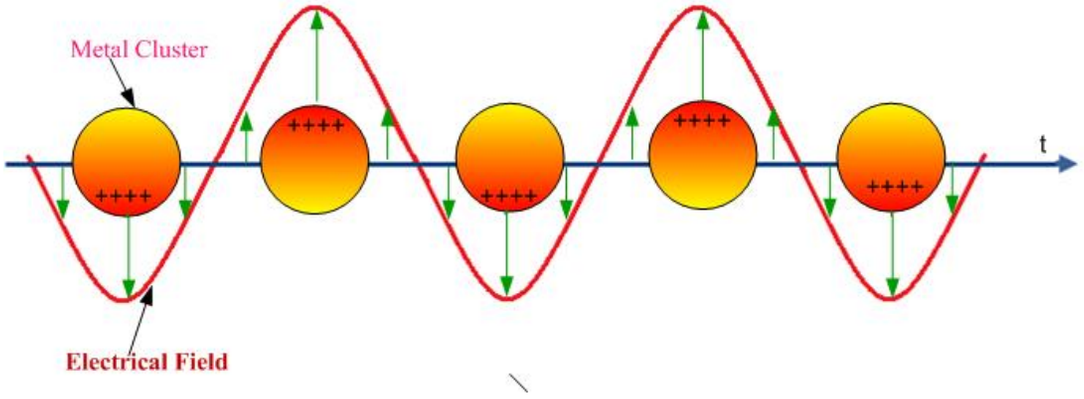


**Figure 5.** Collective Oscillations of free electrons due to applied electric field

The optical resonance related to these oscillations is called the localized SPR (LSPR) [20]. The origin of the term "surface" comes from the knowledge that the oscillations are caused by the polarization of the particle surface, and because the generated electric field is larger near the particle surface and decays farther away far from the surface, which makes that field similar to the evanescent field at a flat interface in the propagating SPR case. In the general case, the frequency of the collective oscillations does not coincide with the applied wave frequency and is determined by many factors, electron concentration, electron effective mass, the particle shape and size, interaction between the particles, and the influence of the environment. However, for an elementary description of the nanoparticles plasmon resonance it is sufficient to use the usual dipole approximation, and the Drude model. The electrostatic polarizability of particle $\alpha_0$ [20] assigns the scattering and absorption of light by a small particle. The electrostatic polarizability of the particle can be calculated using the metal optical permittivity $\varepsilon_m$, the medium dielectric constant $\varepsilon_d$, and the particle geometrical dimensions [20, 40]:

$$\alpha_0 = a^3\left(\frac{\varepsilon_m - \varepsilon_d}{\varepsilon_m + 2\varepsilon_d}\right) \quad (47)$$

Moreover, static polarizability is [20]

$$\alpha = \frac{a\alpha_0}{a - (k^2 + 0.67ik^3a)\alpha_0} \tag{48}$$

Where

$$k = \frac{2\pi\sqrt{\varepsilon_d}}{\lambda}$$

is the medium wave number. The fundamental assumption in the theoretical model is that of a spherical particle shape, which allows us to utilize extended the Mie theory. Furthermore, we can assume that the particles are distributed in a triangular two-dimensional array instead of in a disordered layer. This assumption allow us to perform efficient estimates of the inter particle coupling effects. The calculated quantity is the extinction cross-section, which is formally obtained from the integral [41]:

$$C_{ext} = \frac{1}{2I_0}\mathrm{Re}\int_A \left[ E_i \times H_s^{\dagger} + E_s \times H_i^{\dagger} \right] \cdot \hat{n} dA \tag{49}$$

Here, ( $E_i(r)$ , $H_i(r)$ ) and ( $E_s(r)$ , $H_s(r)$ are the incident and total scattered fields, respectively, and $I_0$ is the incident irradiance. The integral is evaluated over an arbitrary surface A that encloses the entire nanoparticle system. In the case of an isolated spherical nanoparticle illuminated by a plane wave, the scattering cross-sections $C_{ext}$ are calculated based on the Mie scattering theory [42]. From Eqs.(47) and (49) and badi the scattering cross-sections is[20]

$$C_{ext} \cong 4\pi k \,\mathrm{Im}(\alpha) \tag{50}$$

In the static case the extinction cross-section will be [43] explained by Eq (50). One can see from the latter expression that the extinction spectrum has a strong resonance when:

$$\varepsilon_m(\omega = \omega_{res}) = -2\varepsilon_d \tag{51}$$

The permittivity of bulky metal is explained by the Drude model; hence, we utilize it to obtain the resonance frequency:

$$\varepsilon_m(\omega) = \varepsilon_{ib} - \frac{\omega_p^2}{\omega(\omega + i\gamma_b)} \tag{52}$$

where $\varepsilon_{ib}$ is the contribution of the inter band electronic transitions and $\gamma_b$ is the volume decay constant. The metal permittivity is a main parameter for determining the LSPR frequency. So, we consider the exact Drude model. From Eq. (51) and Eq. (52) making the assumption that the significant contribution to the extinction spectrum is caused by absorption, the effective absorption cross-section can be expressed by the resonance frequency as follows

$$C_{abs} = \frac{12\pi k}{a^3}\frac{\varepsilon_d \,\mathrm{Im}(\varepsilon_m)}{\left|\varepsilon_m - \varepsilon_d\right|^2}\times\left|\alpha\right| = \pi a^2 \frac{12\cdot k\cdot a\cdot \varepsilon_d}{(2\varepsilon_d + \varepsilon_{ib}^2)}\times\frac{\omega_p^2(\gamma_b/\omega)(\omega+\gamma_b)^2}{(\omega^2+\gamma_b^2-\omega_{res}^4)^2+\omega_{res}^4\times(\gamma_b^2/\omega^2)} \tag{53}$$

The resonance frequency and resonance wavelength are given by [20]

$$\omega_{res} = \frac{\omega_p}{\sqrt{\varepsilon_{ib}+2\varepsilon_d}} \quad \lambda_{res} = \lambda\sqrt{\varepsilon_{ib}+2\varepsilon_d} \tag{54}$$

where

$$\omega_{res}\,,\ \lambda_{res}\ \text{ and }\ \lambda_p = \frac{2\pi c}{\omega_p}$$

are the resonance frequency, resonance wavelength and plasma wavelength respectively, demonstrated as [44, 45] that is near the resonance, and sometimes for comparison between the metallic bulk permittivity and the metallic nano particle permittivity, the absorption spectrum can be approximately reduced to a Lorenzian profile.

The wavelength modulation is the common method used for LSPR sensor. So, it is the shift in the maximum (or minimum) of the spectrum curve that is monitored as a function of changes in the local dielectric environment that is caused by analyte absorption. The mechanism of this method is described in Eq. (48), and it has been demonstrated for variation of refractive index or the length of a molecular which was adsorbed to receptor. In this equation, the sensitivity to the bulk refractive index ( $S_{\lambda\to bulk}$ ) plays an important role in determining the total response of the LSPR. This sensitivity depends on various factors such as the size and shape of the nanoparticles. In the following section, we discuss the effect of the shape and design of the particle on the sensing process. Apparently, the resonance position is not dependent on the particle size as can be seen by Eq. (54) for a sphere and Eq. (50) for an arbitrary smooth particle and only variation in the intensity of the SPR band with particle size is observed. However, experimentally the SPR bandwidth as well as the band position is observed depending on the nanoparticle size. In the modification to the Mie theory, Drude and Sommerfeld considered that the relative permittivity of the nanoparticle depends on the size $\varepsilon(\omega, R)$ in lieu of $\varepsilon(\omega)$ . The real and the imaginary parts of the modified relative permittivity are given by [46, 47]:

$$\varepsilon'(\omega) = \varepsilon_{ib} - \frac{\omega_p^2}{\omega^2-\omega_d^2} \quad \text{and} \quad \varepsilon''(\omega) = \frac{\omega_p^2\times\omega_d}{\omega(\omega^2+\omega_d^2)} \tag{55}$$

Where $\varepsilon_{ib}$ is the high-frequency limit of $\varepsilon(\omega)$ , arising from the response of the core electrons (electrons in completely filled bands); $\omega_d$ is the relaxation or damping frequency that represents collisions of electrons with the lattice (phonons) and defects; and $\omega_d$ is the bulk plasmon frequency. Dependence of the relative permittivity on the particle radius $R$

was introduced by assuming that the particle size is smaller than the mean free path of the conduction electrons. The damping frequency $\omega_d$ is related to the mean free path of the conduction electrons in the bulk metal $R_{bulk}$ and the Fermi velocity of electrons $\upsilon_f$ by:

$$\omega_d = \frac{\upsilon_f}{R_{bulk}} \tag{56}$$

When $R$ becomes smaller than the mean free path, surface scattering is dominant. Such surface scattering results in the peak broadening and induces a $1/R$ dependence of the SPR bandwidth. In this case, the mean free path $R_{eff}$ becomes size-dependent according to:

$$\frac{1}{R_{eff}} = \frac{1}{R} + \frac{1}{R_{bulk}} \tag{57}$$

One can see from the above equations that the metal particle's shape dictates the spectral signature of its plasmon resonance; the ability to change this parameter and study the effect on LSPR response is a very important experimental challenge. The development of increasingly sophisticated lithographic and chemical methods now allows for the routine production of a wide variety of complex NPs and their assemblies [50].

### 4.3. Metal cluster

The intraction of light with the metal cluster is the atractive aspect in nanotechnology. The electrons between metal atoms in small clusters are localized, and the plasmon resonance is a size dependent phenomenon.

The absorption and scattering cross section $C_{abs}$ and $C_{sca}$ are the common parameter to express the optical properties. Hence, absorption and scattering particles are not purely, so extinction cross section should be considered, which is the sum of both $C_{abs}$ and $C_{sca}$ or and $C_{ext} = C_{abs} + C_{sca}$. In the quasi-static the metal cluster is a spherical form with the radius is smaller than the wavelength ($R << \lambda$). On the other hand, extinction cross section may be written in other form as follows:

$$C_{ext}(\omega) = 9\frac{\omega}{c}\varepsilon_m^{3/2} V_0 \frac{\varepsilon_2(\omega)}{\left[\varepsilon_1(\omega) + 2\varepsilon_m\right]^2 + \varepsilon_2^2(\omega)} \tag{58}$$

Where $\omega/c$, $V_0$, $\varepsilon_m$ and $\varepsilon(\omega)$ are the wave vector, cluster volume, dielectric function of the embedding medium and dielectric function of the particle metal. The extinction cross section is due to dipolar absorption.

A multidipolar contribution, quadrupole extinction and quadrupole scattering are conquered in the scattering cross section in this region. Consequantly, the position and shape of the plasmon resonance will depend on the size, the dielectric functions of the metal clusters, the dielectric function of the surrounding medium and the shape of the particles, its aggregations and, interactions with the substrate etc..

### 4.4. The nanoparticle in liquid matrix

Today, any investigation of nano-fluid is considerable. Hence, in this instance, the complex refractive index of liquids containing isotropic nanoparticles and optical the response of medium are investigated. The diameter of the particles is much smaller than the wavelength of the incident light. The response of a medium to an external electromagnetic field cannot be completely described using macroscopic fields as local field effects play an important role. This pont was first demonstrated by Lorentz who showed an impressive accuracy when predicting the dielectric function of the medium [49]. The external field induces a collection of dipole moments [50] and the local field factor relates the macroscopic fields to the local ones. These local field factors are important in the derivation of various effective medium theories (EMTs) considered next here. Regardless of the composition of the nanocomposite, the effective dielectric function can always be estimated by Wiener [51]

$$\varepsilon_{eff}(\omega) \le \sum_{i=1}^{N} f_i \varepsilon_i(\omega) \ , \ \frac{1}{\varepsilon_{eff}(\omega)} \le \sum_{i=1}^{N} \frac{f_i}{\varepsilon_i(\omega)} \tag{59}$$

where the summation is more than the number of constituents $N$, and their corresponding volume fractions $f_i$ and complex dielectric functions $\varepsilon_i(\omega)$. These limits correspond to capacitors that are connected in parallel or as a series *i.e.* the Wiener bounds give upper and lower limits for the effective complex dielectric function for a certain volume fraction irrespective of the geometry of the nanostructure. Even tighter limits, such as Hashin–Shtrikman and Bergman–Milton, can be utilized in the estimation of the effective dielectric function for two-phase nanocomposites with known volume fractions of the constituents [51–54]. For a more detailed description of the different models see, *e.g.*, a review article by Hale [55].

The Maxwell Garnet (MG) EMT can be used to describe the effective dielectric function of a solution containing a small number of spherical nanoparticles. This dilute limit must be assumed as the MG model itself does not include interaction between nanoparticles or agglomeration. In such a case the effective dielectric function of a medium is given by

$$\frac{\varepsilon_{eff}(\omega) - \varepsilon_h(\omega)}{\varepsilon_{eff}(\omega) + 2\varepsilon_h(\omega)} = f_i \frac{\varepsilon_i(\omega) - \varepsilon_h(\omega)}{\varepsilon_i(\omega) + 2\varepsilon_h(\omega)} \tag{60}$$

where $\varepsilon_i(\omega)$ and $\varepsilon_h(\omega)$ are the frequency-dependent complex dielectric functions of the inclusions and the host, respectively. Naturally the corresponding volume fractions $f_i$ and satisfy $f_i + f_h = 1$. The predicted optical properties of an MG medium are in fine agreement with the measured ones/properties for relatively low volume fractions of the inclusions.

Mathematically this low volume fraction limit of the MG formalism arises from the asymmetric equation for the effective dielectric function since the effective dielectric function would become dependent on the choice of the host material for a two-phase MG system with comparable volume fractions. The Bruggeman effective medium theory (BMT) [56] is based on the assumption that the inclusions are embedded in the effective medium

itself, which is invariant if the constituents are replaced by each other. The Bruggeman formalism has been extended to inclusions with non-spherical shape by introducing a geometric (or depolarization) factor $g$ [57], which depends on the shape of the inclusions. This generalized BMT is

$$f_h \frac{\varepsilon_h(\omega) - \varepsilon_{eff}(\omega)}{\varepsilon_h(\omega) + g[\varepsilon_h(\omega) - \varepsilon_{eff}(\omega)]} + f_i \frac{\varepsilon_i(\omega) - \varepsilon_{eff}(\omega)}{\varepsilon_i(\omega) + g[\varepsilon_i(\omega) - \varepsilon_{eff}(\omega)]} = 0 \tag{61}$$

For example, the classical Bruggeman formula is obtained with a value of g = 1/3 which corresponds to spherical inclusions whereas for two-dimensional circular inclusions the value of g = 1/2. Thus by extracting the effective dielectric function of a two-phase nanocomposite with known volume fractions and dielectric functions of the constituents, we can solve 10 for $g$ and then obtain the geometrical shape of the investigated particles.

The quadratic Eq. (61) has two solutions for the complex effective dielectric function but only the positive branch of the square root is physically reasonable and is given by

$$\varepsilon_{eff}(\omega) = \frac{-c(\omega) + [c^2(\omega) + 4g(1-g)\varepsilon_h(\omega)\varepsilon_i(\omega)]^{1/2}}{2(1-g)} \tag{62}$$

Where

$$c(\omega) = 3(f_h - 1)\varepsilon_h(\omega) + (3f_i - 1)\varepsilon_i(\omega) \tag{63}$$

The frequency-dependent effective refractive index $n_{eff}(\omega)$ and the effective extinction coefficient $k_{eff}(\omega)$ keff(ω) of a nanoliquid are connected to effective dielectric function $\varepsilon_{eff}(\omega)$ as follows:

$$n_{eff}(\omega) = \frac{1}{\sqrt{2}}[\mathrm{Re}\{\varepsilon_{eff}\} + (\mathrm{Re}\{\varepsilon_{eff}\}^2 + \mathrm{Im}\{\varepsilon_{eff}\}^2)^{1/2}]^{1/2} \quad k_{eff}(\omega) = \frac{\mathrm{Im}\{\varepsilon_{eff}\}}{2n_{eff}} \tag{64}$$

We show in Figure 4.4 the effective dielectric functions for MG and BR type curves with geometric factors g = 1/3 and g = 1/2, which are inside the Wiener bounds as expected.

Further, at low volume fractions these three curves are almost overlap, whereas there is a rather larger difference for larger volume fractions. Hence it is important to know how to model the medium with nanoparticles to gain an accurate retrieval of the complex refractive index of an individual nanoparticle. Before closing this section we want to mention that the MG model can be generalized to hold for ellipsoids [58] by using a geometric factor such as that for BR [59]. The calculation of this geometric factor $g$ for ellipsoids can be found from [60].

In the Rayleigh limit $r_0 << \lambda$ , the optical intensity at SPR resonance decays approximately as $I \propto \left(\frac{r_0}{r}\right)^6$ where r is the distance from the center of the metal particle. We can use this

dependence in order to define an effective refractive index of the medium surrounding the metal core according to:

$$n_{eff} = \frac{n_2 \int_{r_0}^{r_0+d} 4\pi r^2 \left(\frac{r_0}{r}\right)^6 \partial r + n_1 \int_{r_0+d}^{\infty} 4\pi r^2 \left(\frac{r_0}{r}\right)^6 \partial r}{\int_{r_0}^{\infty} 4\pi r^2 \left(\frac{r_0}{r}\right)^6 \partial r} = n_2 - \frac{n_2 - n_1}{\left(1 + \left(\frac{d}{r_0}\right)^3\right)} \tag{65}$$

## 5. SPR sensor parameters

The main performance parameters of SPR sensors for nano application are sensitivity, linearity, resolution, accuracy, reproducibility and limitation of detection.

*Sensitivity*

Sensor sensitivity is the ratio of the change in the sensor output to the change in the refractive index [1].

$$S = \frac{\partial Y}{\partial n} \tag{66}$$

S , $Y$ and $n$ are the sensitivity, sensor output and refractive index of the probe medium respectively.

*Sensor linearity*

Sensor linearity is related to linear relationship of output sensor to quantity which should be measured.

*Resolution and Reproducibility*

The resolution of a sensor is the smallest change in the measured quantity which produces a detectable change in the sensor output. The resolution of SPR sensor usually refers to a bulk refractive index resolution. In SPR biosensor, an equivalent of this term is the limit of detection. Sensor accuracy describes the closeness of agreement between the measured quantity and the true value of the quantity such as refractive index or concentration of the analyte. It is usually expressed in absolute terms or as a percentage of the error/output ratio.

Reproducibility is the ability of a sensor to provide the same output when measuring the same value of the quantity measurement such as concentration or refractive index under the same operating condition over a period of time. It is expressed as the percentage of full range. The limitation of detection is an important parameter for evaluation of sensor. It is related to minimum detection of concentration of analyte. The minimum variation of quantity which measured with the sensor is related to minimum concentration value which is expressed the limitation detection.

## 6. Simulation of SPR Curve for various refractive index

Figure 6 shows the simulation of SPR curve for variation of the refractive index of analyte. The refractive index of prism and gold layer are 1.83 and .235+3.31i respectively. The wavelength of incident light was 632.8 nm (He-Ne Laser). When the incident angle was changed from 30º to 90º the refractive index of analyte shifted from 1.1 up to 1.6. Figure 7 shows the resonance angle shifted from 39.76º to 80.24º. Moreover, in accordance with Figures 8 and 9, the changes in refractive index are 0.01 and 0.001 respectively. As a result, the resonance angle shifts for small variation of refractive index of analyte are 10.944 and 0.08 respectively [61].

Figure 10 shows the variation of reflectivity with refractive index of analyte. Consequently, the reflectivity increased with increasing refractive index of analyte.

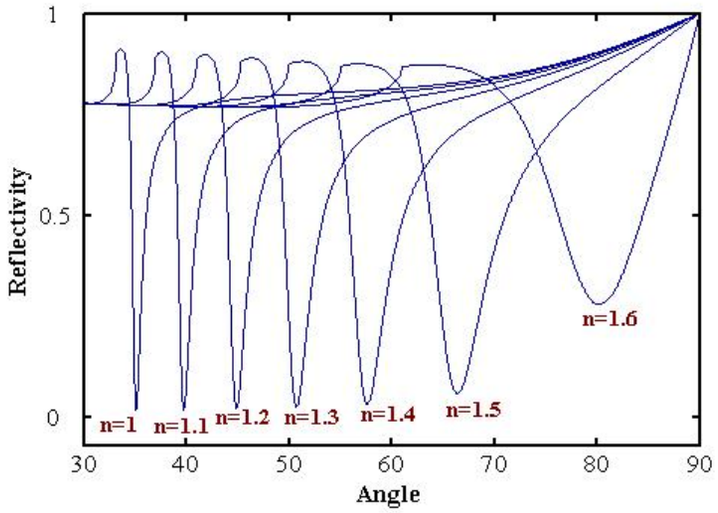


**Figure 6.** Simulation of SPR curve for various refractive index of analyte from 1.1 to 1.6[61]

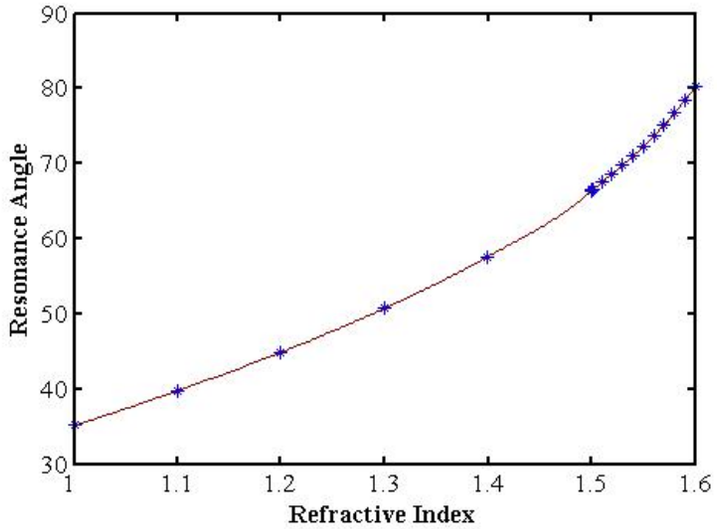


**Figure 7.** The variation of resonance angle with refractive index of analyte[61]

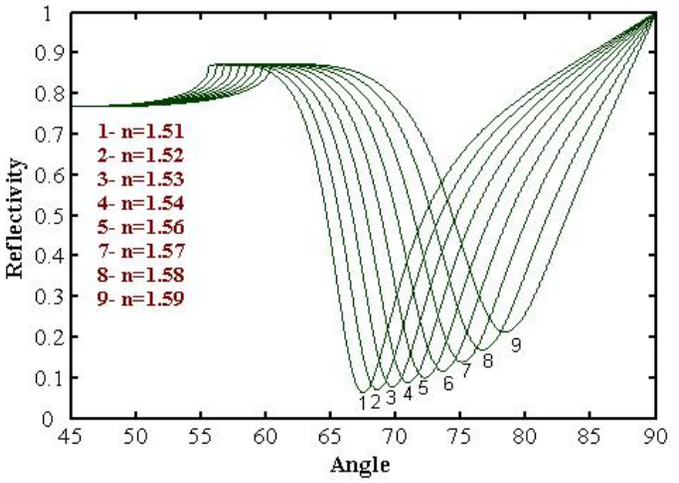


**Figure 8.** Simulation of SPR curve for various refractive index of analyte from 1.51 to 1.59[60]

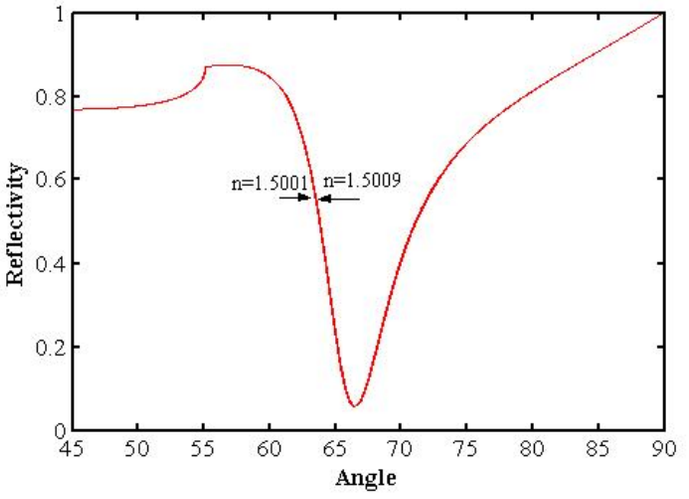


**Figure 9.** Simulation of SPR curve for variation of refractive index of analyte for 1.5001 and 1.5009[61]

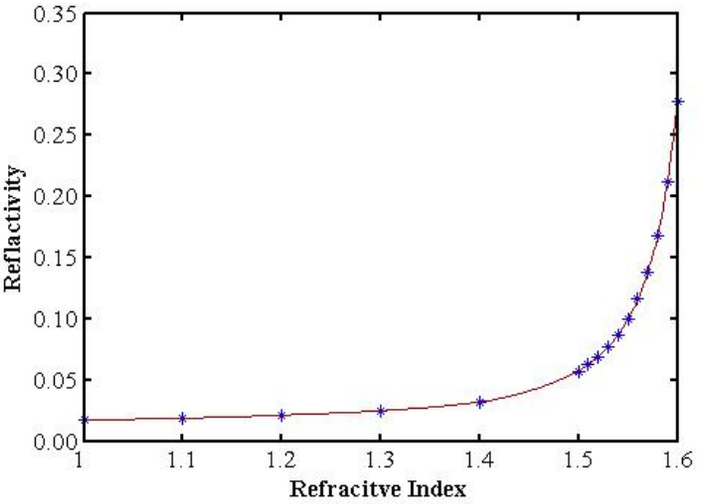


**Figure 10.** Reflectivity with refractive index of analyte[61]

If the nano-fluid is considered, the refractive index of analyte has an imaginary part which is changed from 0.001 to 0.2, and the resonance angle and reflectivity are shifted from 52.34º to 54.628º and .0252 to 0.6587 respectively, that are depicted in figure 11.

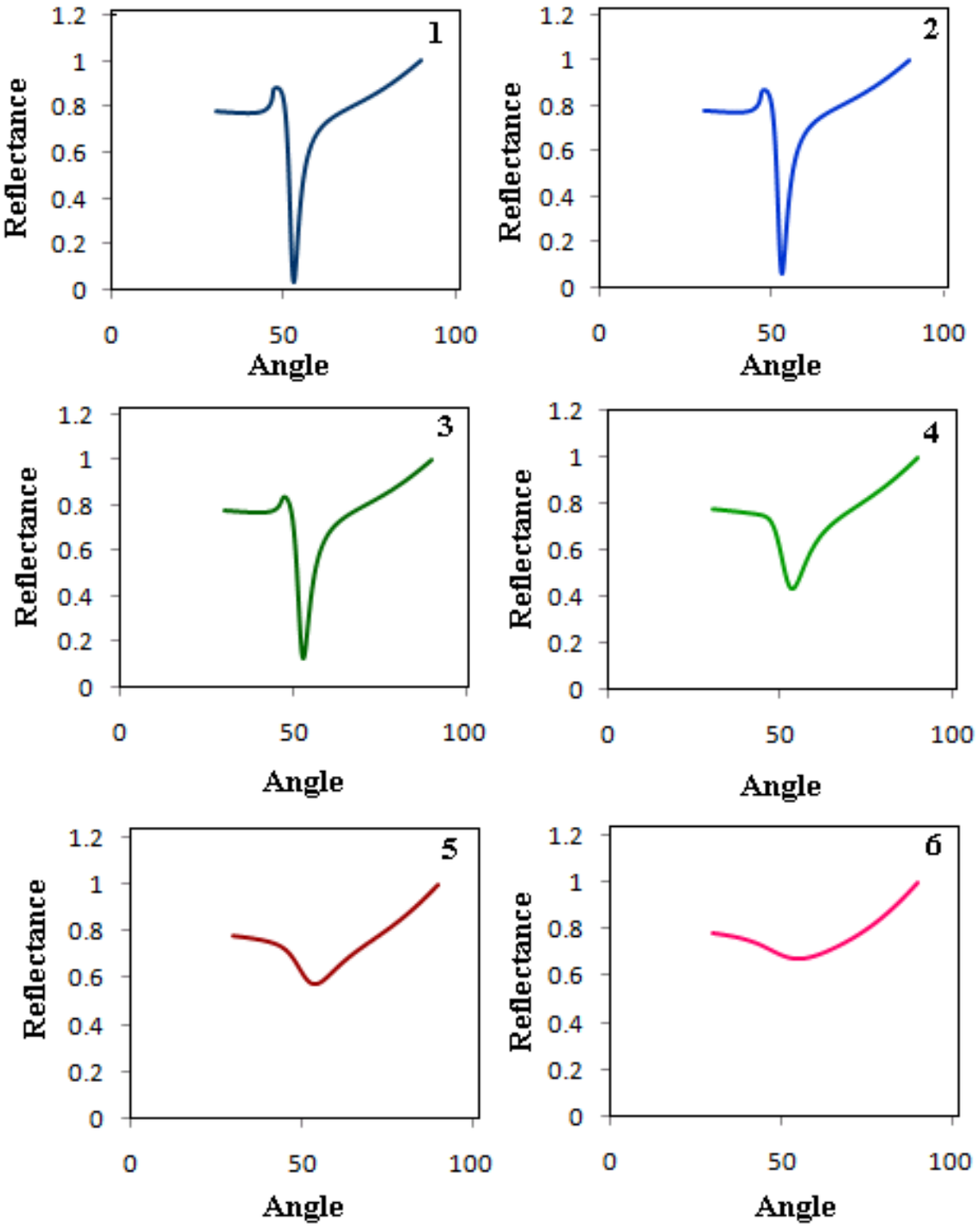


**Figure 11.** SPR signals related to simulation of nano fluid

The pertinent parameters were sorted in Table 1. Figure 12a and 12b show the variation of resonance angle and reflectivity versus the imaginary part.

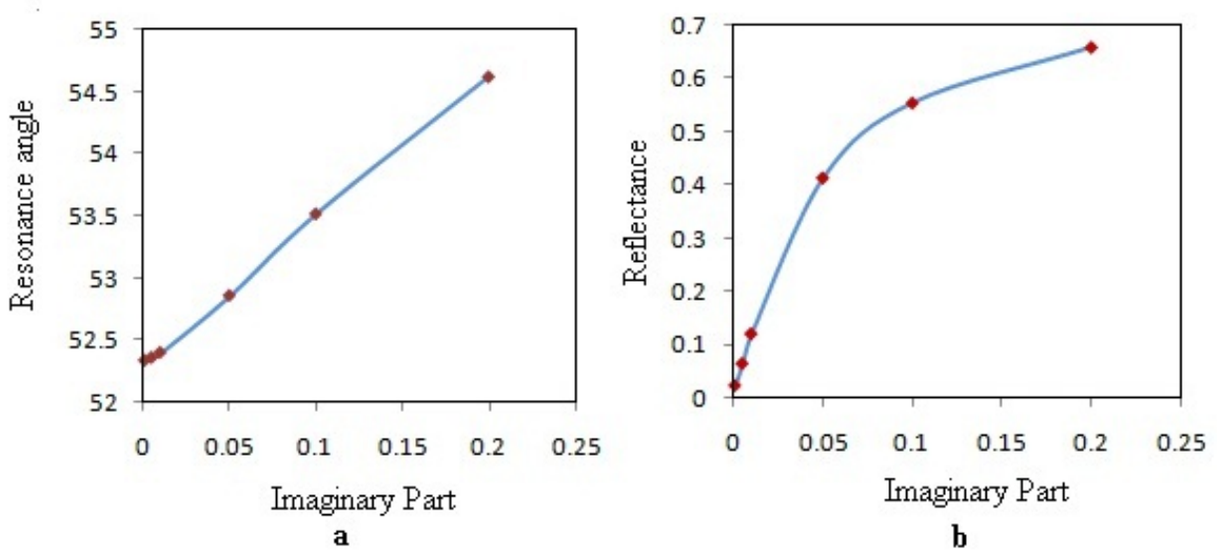


**Figure 12.** Variation of resonance angle and reflectance versus the imaginary part of liquid

| Refractive index | Resonance angle | Reflectance |
|---|---|---|
| 1.331+0.001i | 52.34 | 0.0252 |
| 1.331+0.005i | 52.364 | 0.0663 |
| 1.331+0.01i | 52.405 | 0.1221 |
| 1.331+0.05i | 52.864 | 0.4140 |
| 1.331+0.1i | 53.523 | 0.5546 |
| 1.331+0.2i | 54.628 | 0.6587 |

**Table 1.** Pertinent parameters for simulation of nanofluid

## 7. Application of SPR nano-metal

One of the most attractive aspects of collective excitations of Plasmon is their use to concentrate light in sub wavelength structures and enhance transmission through periodic arrays of sub wavelength holes in optically thick metal films. SPs are tightly bound to metal–dielectric interfaces penetrating around 10 nm into the metal (the so-called skin depth) and typically more than 100 nm into the dielectric (depending on the wavelength). SPs at the optical wavelengths concentrate light in a region that is considerably smaller than their wavelength, a feature that suggests the possibility of using surface – plasmon polaritons for the fabrication of nanoscale photonic circuits operating at optical frequencies. In addition the possibility of manufacturing such nano beds in planar form makes them remarkably important for biosensing towards biochip application.

Aslan et. al., reported on Nanogold-plasmon-resonance-based glucose sensing in 2004 [62]. Their sensor based on the aggregation and disassociation of 20-nm gold particles. The plasmon absorption was shifted due to interaction of nanoparticle and glucose and the response range is $\mu M \rightarrow mM$ glucose levels in many biological sample.

Application of Au nanocluster-embedded film was reported by Hu, et. al. in 2004 [6]. The used the mentioned dielectric film ($SiO_2$) in biosensor and prepared a novel ultrahigh-resolution surface plasmon resonance biosensor. The limitation of sensor was reported 0.1 pg/mm$^2$ and this sensor can detect the interaction of small molecules in low concentrations. The sensitivity of sensor depend on the size and volume fraction of the embedded Au nanoclusters [6].

Another application of gold nanoparticle in SPR sensor was reported by Chau et al in 2006 [63]. A novel localized surface plasmon resonance based on fiber-optic was used for sensing $Ni_2^+$ ion and label-free detection of streptavidin and staphylococcal enterotoxin B at the picomolar level using self-assembled gold nanoparticles [63].

In order to develop the fully integrated portable surface plasmon resonance (SPR) system for detection of explosives, the amplification strategy of SPR signal was investigated. Indirect competitive inhibition method allowed the middle-sized SPR sensor to detect trinitrotoluene (TNT) at ppt level [64]. However, this enhanced SPR signal was not high enough to detect TNT at ppt level by a miniaturized SPR sensor. Therefore, localized surface plasmon resonance (LSPR) effect using Au nanoparticle as further signal amplification approach was used. The amplification method of indirect competitive inhibition and LSPR were combined together for fabrication of the immunosurface using Au nanoparticle. TNT detectable range of this immune surface was from 10 ppt (10 pg/ml) to 100 ppb (100 ng/ml), which was almost comparable to that without Au nanoparticle. The observed resonance angle change due to binding monoclonal TNT antibody (M-TNT Ab) with the immune surface modified with Au nanoparticlewas amplified to four times higher than that in absence of Au nanoparticle [64].

LSPR sensors and silver nanoparticle were applied with various thiolate self-assembled monolayers (SAM) to provide chemical selectivity for detection of volatile organic compounds (VOCs) [65]. LSPR spectrums of silver nanoparticles were shifted due to binding and for detection should be measured as the response signal. The limitation of sensor detection was as low as 18–30ppm for heptanone, depending on the surface modification of Ag nanoparticles [65].

Moreover for colorimetric hydrogen peroxide, the LSPR of poly(vinylalcohol) capped silver nanoparticles was used [66]. The silver nanoparticles are directly synthesized in the PVA matrix treatment in aqueous medium. No other reagent is used. . The silver nanoparticles have the catalytic ability for the decomposition of hydrogen peroxide; then the decomposition of hydrogen peroxide induces the degradation of silver nanoparticles. Hence, a remarkable change in the localized surface plasmon resonance absorbance strength could be observed. As a result, the yellow color of the silver nanoparticle–polymer solution was gradually changed to transparent colour. Furthermore, when this transparent solution was subjected to thermal treatment, it became again yellow and the UV–vis spectroscopy confirmed that nanoparticles were again formed, suggesting the renewability of this sensor. The determination of reactive oxygen species such as hydrogen peroxide has possibilities for applying to medical and environmental applications [66].

Salmonella was detected using LSPR and Au nanoparticles [67]. In this case, the small contact area between the nanoparticle and the bacteria was the cause of the short range interaction of the local electric field and bacteria. Hence, the SPR signals were shifted to higher value that can be explained by the Mie theory and effective medium theory. So, this is alternative methods for detection of Salmonella [67].

## Author details

Amir Reza Sadrolhosseini
*Center of Excellence for Wireless and Photonics Networks (WiPNet), Faculty of Engineering Universiti Putra Malaysia, UPM Serdang, Malaysia*

A. S. M. Noor
*Center of Excellence for Wireless and Photonics Networks (WiPNet), Faculty of Engineering Universiti Putra Malaysia, UPM Serdang, Malaysia*
*Department of Computer and Communication Systems Engineering, Faculty of Engineering, Universiti Putra Malaysia, UPM Serdang, Malaysia*

Mohd. Maarof Moksin
*Department of Physics, Faculty of Science, Universiti Putra Malaysia, Serdang, Malaysia*

## 8. References

[1] Homola J. Surface plasmon resonance based sensors. Verlag Berlin Heidelberg: Springer; 2006.
[2] Peyghambarian N, Koch S W, Mysyrowicz A. Introduction to Semiconductor Optics. New Jersey: Prentice Hall; 1993.
[3] Liedberg, B., Nylander, C., Lundstrom, I. 1983. Surface plasma resonance for gas detection and biosensing. Sensors and Actuators B 1983; 4 299.
[4] Stenberg E, Persson B, Roos H, Urbaniczky, C. Quantitative determination of surface concentration of proteins with surface plasmon resonance using radiolabeled protein. J. Colloid. Interf. Sci. 1991; 143 513–526.
[5] Homola J, Yee S, Gauglitz G. Surface plasmon resonance sensors: review. Sens. Actuat. B 1999; 54 3–15.
[6] Hu W, Chenb S-J, Huangc K-T, Hsud J H, Chend W Y, Changa G L, Lai K-A. A novel ultrahigh-resolution surface plasmon resonance biosensor with an Au nanocluster-mbedded dielectric film. Biosensors and Bioelectronics 2004;19 1465–1471.
[7] Zhu T, Zhang X, Wang J, Fu X, Liu Z . Assembling colloidal Au nanoparticles with functionalized self-assembled monolayers. Thin Solid Films 1998; 327–329 595–598.
[8] Gradar K C, Brown K R, Keating C D, Stranick S J, Tang S-L, Natan M J. Nanoscale characterization of gold colloid monolayers: a comparison of four techniques. Anal. Chem. 1997;69 471–477.

[9] Brown K R, Lyon L A, Fox A P, Reiss B D, Natan M J. Hydroxylamine seeding of colloidal Au nanoparticles. Part 3. Controlled formation of conductive Au films. Chem. Mater. 2000; 12 314–323.

[10] Lyon L A, Musick M D, Natan M J. Colloidal Au-enhanced surface plasmon resonance immunosensing. Anal. Chem. 1998; 70 5177–5183.

[11] He L, Musick M D, Nicewarner S R, Salinas F G, Benkovic S J, Natan M J, Keating C D. Colloidal Au-enhanced surface Plasmon resonance for ultrasensitive detection of DNA hybridization. J. Am. Chem. Soc. 2000; 122 9071–9077.

[12] Gestwicki J E, Hsieh H V, Pitner J B. Using receptor conformational change to detect low molecular weight analytes by surface plasmon resonance. Anal. Chem. 2001; 73 5732–5737.

[13] Sun Y, Xia Y. Increased sensitivity of surface plasmon resonance of gold nanoshells compared to that of gold solid colloids in response to environmental changes. Anal. Chem. 2002; 74 5297–5305.

[14] Mayer C, Stich N, Schalkhammer T, Bauer G. Slide-format proteomic biochips based on surface-enhanced nanocluster-resonance. Fresenius J. Anal. Chem. 2001; 371 238–245.

[15] Kouzani A Z, Dai X J, Michalski W P. Investigation of the effect of design parameters on sensitivity of surface plasmon resonance biosensors. Biomedical Signal Processing and Control - Biomed Signal Process Control 2011 6( 2) 147-156, 2011.

[16] Wang J. Carbon-nanotube based electrochemical biosensors: a review. Electroanalysis 2005; 17 7–14.

[17] Balasubramanian K, Burghard M. Biosensors based on carbon nanotubes, Analytical and Bioanalytical Chemistry 2006; 385 452–468.

[18] Liu Y, Koep E, Liu M. A highly sensitive and fast-responding SnO2 sensor fabricated by combustion chemical vapor deposition. Chemistry of Materials 2005; 17 3997–4000.

[19] Choi A, Kim K, Jung H-I, Lee S Y. ZnO nanowire biosensors for detection of biomolecular interactions in enhancement mode. Sensors and Actuators B: Chemical 2010; 148 577–582.

[20] Zalevsky Z, Abdulhalim I. Integrated nanophotonics devices Elsevier Science 2010.

[21] Willets K A, Van Duyne R P. Localized Surface Plasmon Resonance Spectroscopy and Sensing. Annu. Rev. Phys. Chem. 2007; 58:267–97.

[22] Kittle C. Solid State Physics New York: Wiley; 1996.

[23] Sosa I O, Noguez C, Barrera R G. Optical Properties of Metal Nanoparticles with Arbitrary Shapes. J. Phys. Chem. B 2003; 107 6269-6275.

[24] Kelly K L, Lazarides A A, Schatz G C. Computational electromagnetics of metal nanoparticles and their aggregates. Computing in Science and Engineering, 2001; 3( 4) 67.

[25] Mishchenko M I, Hovenier J W, Travis L D. Light Scattering by Nonspherical Particles. San Diego: Academic Press; 2000.

[26] Toma H E, Zamarion V M, Toma S H, Araki K. The coordination chemistry at gold nanoparticles J. Braz. Chem. Soc. 2010; 21(7).

[27] Draine B T. Astrophys. J. 1998; 333 848.
[28] Draine B T, Flatau P J. Program DDSCAT; University of California at San Diego: San Diego, CA.
[29] Johnson P B, Christy, R. W. Phys. ReV. B 1972; 6 4370.
[30] Yang W-H, Schatz G C, van Duyne R P. Discrete dipole approximation for small particles with arbitrary shapes. J. Chem. Phys. 1995; 103 869.
[31] Jensen T R, Duval M L, Kelly K L, Lazarides A A, Schatz G C, Van Duyne, R P. Nanosphere lithography: Effect of the external dielectric medium on the surface plasmon resonance spectrum of a periodic array of silver nanoparticles, Journal of Physical Chemistry B, 1999; 103(45) 9846 – 9853.
[32] Noguez C, Sosa I, Barrera R G. Optical characterization of isolated nanoparticles with arbitrary shapes MRS Proc. 2002; 704 275.
[33] Noguez C, Sosa I, Barrera R G. MRS Proc. 2002, 704, 275; Singh, R. K., Partch, R., Muhammed, M., Senna, M., Hofmann, H., Eds.
[34] Fontana E. Thickness Optimization of Metal Films for the Development of Surface Plasmon Based Sensors for non-absorbing media. Journal of Applied optics 2006.
[35] Schasfoort, R. and Tudos, A. 2008, Handbook of Surface Plasmon Resonance. RSC Publishing, Cambridge, U.K.
[36] Sharma K. 2006. Optics. Academic Press, California, 301-316.
[37] Beketov G V, Shirshov Y M, Shynkarenko O V, Chegel V I. Surface plasmon resonance spectroscopy: prospects of superstrate refractive index variation for separate extraction of molecular layer parameters. Sensors and Actuators B. 1998; 48 432.
[38] Sadrolhosseini A R, Moksin M M, Yunus W M M, Talib Z A, Abdi M M. Surface Plasmon Resonance Detection of Copper Corrosion of Biodiesel Using Polypyrrole-Chitosan Layer Sensor. Optical review 2011 18(4) 331-337.
[39] Yuan X-C, Ong B, Tan Y, Zhang D, Irawan R, Tjin S. Sensitivity-stability-optimized surface plasmon resonance sensing with double metal layers. Journal of optics 2006; 959 963-8.
[40] Stewart ME, Anderton CR, Thompson LB, Maria J, Gray SK, Rogers JA . Nanostructured plasmonic sensors. Chem Rev 2008;108: 494–521.
[41] Xu H, Kall M. Modeling the optical response of nanoparticle- based surface Plasmon resonance sensors. Sensors and Actuators B 2002; 87 244-249.
[42] Mie G. Beitrage zer optik truber meiden speziell kolloidaler metallosungen. Ann. Phys. (Leipzig) 1908; 25 377–445.
[43] Gupta S, Huda S, Kilpatrick PK, Velev OD. Characterization and optimization of gold nanoparticle-based silver-enhanced immu- noassays. Anal Chem 2007; 79 3810–20.
[44] Baptista P, Pereira E, Eaton P, Doria G, Miranda A, Gomes I. Gold nanoparticles for the development of clinical diagnosis methods. Anal Bioanal Chem 2008; 391 943–50.
[45] Luo PG, Stutzenberger FJ. Nanotechnology in the detection and control of microorganisms. Adv Appl Microbiol 2008;63 145–81.

[46] Bruzzone S, Arrighini GP, Guidotti C. Some spectroscopic proper- ties of gold nanorods according to a schematic quantum model founded on the dielectric behavior of the electron-gas confined in a box. Chem Phys 2003; 291 125–40.
[47] Prodan E, Radloff C, Halas NJ, Nordlander P. A hybridization model for the plasmon response of complex nanostructures. Science 2003; 302 419–22.
[48] Wang H, Brandl DW, Nordlander P, Halas NJ. Plasmonic nanos- tructures: artificial molecules. Acc Chem Res 2007; 40 53–62.
[49] Lorentz H A. -ber die beziehungzwischen der fortpflanzungsgeschwindigkeit des lichtes der k◌rperdichte. Ann. Phys. 1880; 9 641–665.
[50] Sutherland R L. Handbook of Nonlinear Optics New York: Marcel Dekker; 1996.
[51] Hashin Z, Shtrikman S. A variational approach to the theory of the effective magnetic permeability of multiphase materials. J. Appl. Phys. 1963; 33 3125–3131.
[52] Milton G W. Bounds on the complex dielectric constant of a composite material. Appl. Phys. Lett. 1980; 37 300–302.
[53] Bergman D J. Exactly solvable microscopic geometries and rigorous bounds for the complex dielectric constant of a two-component composite material. Phys. Rev. Lett. 1980; 44 1285–1287.
[54] Aspnes D E. Bounds to average internal fields in two-component composites. Phys. Rev. Lett. 1982; 48 1629–1632.
[55] Hale D K. The physical properties of composite materials. J. Mater. Sci. 1976; 11 2105–2141.
[56] Sipe J E, Boyd R W. Nonlinear susceptibility of composite optical materials in the Maxwell Garnett model. Phys. Rev. A 1992; 46 1614–1629.
[57] Zeng X C, Bergman D J, Hui P M, Stroud D. Effective-medium theory for weakly nonlinear composites. Phys. Rev. B 1988; 38 10970–10973.
[58] Cohen R W, Cody G D, Coutts M D, Abeles B. Optical properties of granular silver and gold films. Phys. Rev. B 1973; 8 3689–3701.
[59] Lagarkov A N, Sarychev A K. Electromagnetic properties of composites containing elongated conducting inclusions. Phys. Rev. B 1996; 53 6318–6336.
[60] Grosse P, Offermann V. Analysis of reflectance data using the Kramers–Kronig relations. Appl. Phys. A 1991; 52 138–144.
[61] Sadrolhosseini A R. Surface Plasmon Resonance Characterization Of Biodiesel. PhD thesis. Universiti Putra Malaysia; 2011.
[62] Kadir Aslan K, Lakowicz J R, Geddes C D. Nanogold-Plasmon-Resonance-based glucose sensing. Analytical Biochemistry 2004; 330 145-155.
[63] Chau L K, Lin Y F, Cheng S F, Lin T J. Fiber-optic chemical and biochemical probes based on localized surface plasmon resonance. Sensors and Actuators B 2006; 113 100–105.
[64] Kawaguchi T, Shankaran D R, Kim S J, Matsumoto K, Toko K, Miura N. Surface plasmon resonance immune sensor using Au nanoparticle for detection of TNT. Sensors and Actuators B 2008; 133 467–472.

[65] Chena Y Q, Lub C J. Surface modification on silver nanoparticles for enhancing vapor selectivity of localized surface plasmon resonance sensors. Sensors and Actuators B 2009; 135 492–498.

[66] Filippo E, Serra A, Manno D. Poly(vinyl alcohol) capped silver nanoparticles as localized surface Plasmon resonance-based hydrogen peroxide sensor. Sensors and Actuators B 2009 138 625–630.

[67] Fua J, Park B, Zhaoa Y. Limitation of a localized surface plasmon resonance sensor for Salmonella detection. Sensors and Actuators B 2009; 141 276–283.